microLife, 2024, **5**, uqae022
DOI: 10.1093/femsml/uqae022
Advance access publication date: 6 November 2024
Research Article

Tracking the uptake of labelled host-derived extracellular vesicles by the human fungal pathogen *Aspergillus fumigatus*

Corissa Visser[1,2], Flora Rivieccio[1,2], Thomas Krüger[1], Franziska Schmidt[1,2], Zoltán Cseresnyés[3], Manfred Rohde[4], Marc Thilo Figge[2,3,5], Olaf Kniemeyer[1], Matthew G. Blango[6,*], Axel A. Brakhage[1,2,5,*]

[1]Department of Molecular and Applied Microbiology, Leibniz Institute for Natural Product Research and Infection Biology—Hans Knöll Institute (Leibniz-HKI), 07745 Jena, Germany
[2]Institute of Microbiology, Friedrich Schiller University, 07743 Jena, Germany
[3]Research Group Applied Systems Biology, Leibniz Institute for Natural Product Research and Infection Biology (HKI), 07745 Jena, Germany
[4]Helmholtz Centre for Infection Research (HZI), 38124 Braunschweig, Germany
[5]Excellence Cluster Balance of the Microverse, Friedrich Schiller University, 07743 Jena, Germany
[6]Junior Research Group RNA Biology of Fungal Infections, Leibniz Institute for Natural Product Research and Infection Biology (Leibniz-HKI), 07745 Jena, Germany
*Corresponding authors. Matthew G. Blango, Junior Research Group RNA Biology of Fungal Infections, Leibniz Institute for Natural Product Research and Infection Biology (Leibniz-HKI), 07745 Jena, Germany. E-mail: matthew.blango@leibniz-hki.de; Axel A. Brakhage, Department of Molecular and Applied Microbiology, Leibniz Institute for Natural Product Research and Infection Biology—Hans Knöll Institute (Leibniz-HKI), 07745 Jena, Germany. E-mail axel.brakhage@leibniz-hki.de
Editor: [Petra Dersch]

Abstract

Extracellular vesicles (EVs) have gained attention as facilitators of intercellular as well as interkingdom communication during host–microbe interactions. Recently we showed that upon infection, host polymorphonuclear leukocytes produce antifungal EVs targeting the clinically important fungal pathogen *Aspergillus fumigatus*; however, the small size of EVs (<1 µm) complicates their functional analysis. Here, we employed a more tractable, reporter-based system to label host alveolar epithelial cell-derived EVs and enable their visualization during *in vitro A. fumigatus* interaction. Fusion of EV marker proteins (CD63, CD9, and CD81) with a Nanoluciferase (NLuc) and a green fluorescent protein (GFP) facilitated their relative quantification by luminescence and visualization by a fluorescence signal. The use of an NLuc fused with a GFP is advantageous as it allows for quantification and visualization of EVs simultaneously without additional external manipulation and to distinguish subpopulations of EVs. Using this system, visualization and tracking of EVs was possible using confocal laser scanning microscopy and advanced imaging analysis. These experiments revealed the propensity of host cell-derived EVs to associate with the fungal cell wall and ultimately colocalize with the cell membrane of *A. fumigatus* hyphae in large numbers. In conclusion, we have created a series of tools to better define the complex interplay of host-derived EVs with microbial pathogens.

Keywords: extracellular vesicles; A549 epithelial cells; nanoluciferase; green fluorescent protein; CD63; CD81; CD9; *Aspergillus fumigatus*

Introduction

Human pathogenic fungi continue to pose a global threat, especially to immunocompromised individuals and those with underlying diseases such as leukemia, chronic obstructive pulmonary disease, or severe influenza, (Köhler et al. 2017, WHO 2022, Denning 2024). In the recent World Health Organization fungal priority pathogen list, the ubiquitously distributed, filamentous saprobe *Aspergillus fumigatus* was added to the critical priority group due to its ability to cause disease ranging from allergic reactions to life-threatening invasive aspergillosis in immunocompromised hosts (Brakhage 2005, van de Veerdonk et al. 2017, Latgé et al. 2019, WHO 2022). *A. fumigatus* typically undergoes propagation through the asexual production of spores called conidia (Latgé et al. 2019). With their small size of only 2–3 µm in diameter and their hydrophobic surface structure, conidia are dispersed through the air and can be easily inhaled. In the lungs, they can reach the alveoli, where they are rapidly cleared by innate immune cells in immunocompetent hosts, but able to germinate, form hyphae, and cause invasive fungal growth in immunocompromised patients (Heinekamp et al. 2015).

During infection, both professional phagocytic immune cells (Lionakis et al. 2023) and lung epithelial cells (Amin et al. 2014, Ewald et al. 2021, Jia et al. 2023) are required for the coordinated clearance of *A. fumigatus* conidia from the lungs. In recent years, extracellular vesicles (EVs) have gained attention for facilitating communication between human cells or between hosts and microorganisms; however, the potential role of host-derived EVs during *A. fumigatus* infection remains largely unexplored. Recently it was shown that upon infection, host polymorphonuclear leukocytes (PMNs) produce EVs distinct from those released during a healthy state and that are able to inhibit *A. fumigatus* conidia and hyphae (Shopova et al. 2020). EVs are a heterogenous group of membrane-delimited vesicles secreted by almost all cell types that play important roles in cell-to-cell communication during physiological and pathological states (Brakhage et al. 2021). Classification of EVs into subtypes is difficult and currently distinction

Received 16 April 2024; **revised** 16 October 2024; **accepted** 4 November 2024

is mostly based on their type of biogenesis, resulting in three primary subgroups named exosomes, ectosomes/microvesicles, and apoptotic bodies (Abels et al. 2016, van Niel et al. 2018, Brakhage et al. 2021). Apoptotic bodies are a heterogenous group of vesicles associated with cell death and are frequently considered a confounding factor in studies of EVs in otherwise healthy cells (Kakarla et al. 2020), and even more challenging to assess during infection situations. Exosomes are produced in the endosomal pathway by invagination and subsequent inward budding and fission of the limiting membrane of endosomes to form intraluminal vesicles (ILVs). During the maturation process from early to late endosomes, these structures accumulate several ILVs, leading to the generation of multivesicular bodies (MVBs). MVBs are then either directed to lysosomes for degradation of their contents or fused with the cell cytoplasmic membrane releasing the ILVs as exosomes into the extracellular space. Ectosomes are formed through direct outward budding and fission of the cytoplasmic membrane (Abels et al. 2016, van Niel et al. 2018, Brakhage et al. 2021). EVs carry a wide variety of cargo molecules that can elicit specific cellular functions in the recipient cell, including proteins, lipids, polysaccharides, and nucleic acids (Yáñez-Mó et al. 2015). In comparison to spontaneously produced EVs, EVs produced by *A. fumigatus*-infected PMNs were shown to be larger in size and exhibit a higher enrichment of the tetraspanin CD63 in their membranes, as well as a more diverse protein cargo and specifically, larger amounts of proteins and peptides displaying antimicrobial activity. Challenging *A. fumigatus* hyphae with such infection-derived EVs resulted in the localization of the EVs to or within the cell wall as well as infrequently to the cytoplasm of the hyphae, which ultimately resulted in the damage and apparent death of the fungus (Shopova et al. 2020).

There are numerous studies on labeling EVs in the literature, either using lipophilic dyes such as DiR (Lázaro-Ibáñez et al. 2021), radionucleotide labelling (Lázaro-Ibáñez et al. 2021), or tagging of proteins commonly associated with EVs (Hikita et al. 2018, 2020, Cashikar et al. 2019, Gupta et al. 2020, Levy et al. 2020, Lázaro-Ibáñez et al. 2021). Many of these methods either enabled the detection and quantification of EVs *in vitro* as well as *in vivo*, or their visualization, whereas others combined different fusion proteins to allow both detection and visualization simultaneously (Shpigelman et al. 2021). In this study, we sought to build on these works by creating a system that would allow for easy detection and visualization of EVs independent of external labelling and thus potential alteration of their behavior. Therefore, we labelled host cell-derived EVs by genetically fusing the commonly accepted EV marker proteins CD63, CD9, and CD81 with a Nanoluciferase (NLuc) luminescence reporter as well as an appropriate fluorescent protein tag. The resulting constructs were transiently transfected into the human lung epithelial cell line A549. EVs isolated from these cells can be detected and visualized through measurement of the luminescence signal in cell culture supernatants and by confocal laser scanning microscopy (CLSM), respectively. We used this system to track host-derived EVs upon coincubation with *A. fumigatus* and revealed robust association of these labeled EVs with fungal hyphae, establishing a system for future dissections of the role of EVs in cross-kingdom delivery of molecules from host to pathogen.

Materials and methods

Culture conditions of microorganisms

A. fumigatus conidia (Table S1) were plated on malt agar (Sigma Aldrich) and incubated at 37°C. On day 5, conidia were collected from plates by adding 10 ml of sterile ultrapure water (dH_2O) to the plate and scraping the conidia off the agar using a disposable T-shaped scraper. The conidia–water suspension was filtered through a 30 µm cell strainer (MACS, Miltenyi Biotec GmbH) for the removal of mycelium. Conidia were washed by centrifugation at 1800 × *g* and 4°C for 5 min followed by removal of the supernatant and resuspension in sterile dH_2O. Conidia were stored at 4°C for no longer than a week before use.

Cell culture

A549 epithelial cells were cultivated in Kaighn's Modification of Ham's F-12 (F-12 K) medium (Gibco) supplemented with 10% (v/v) artificial FCS (FetalClone III; Cytiva) and penicillin/streptomycin to a final concentration of 1%. Cells were seeded into T25 or T75 cell culture flasks at concentrations of 2×10^5 and 3×10^5, or 6×10^5 and 1×10^6 cells per flask and passaged after 4 and 3 days, respectively. Spent media was removed by aspiration and cells were washed using prewarmed Ca^{2+}/Mg^{2+}-free PBS (Gibco). Cells were detached from the cell culture flasks through the addition of trypsin (Thermo Fisher Scientific) and were subsequently incubated at 37°C with 5% (v/v) CO_2 for 5 min followed by gentle tapping of the culture flask to assure the detachment of all cells. Trypsinization was stopped by the addition of FCS-containing F-12 K medium and cells were transferred to a fresh tube. Cell concentrations were determined using the Luna cell counter and cells were seeded into a new culture flask containing prewarmed media for culturing or into plates as needed for the respective experiments. Seeded cells were incubated at 37°C and 5% (v/v) CO_2. If required, cells were seeded in EV-depleted medium consisting of F-12 K medium supplemented with 1% (v/v) EV-depleted FCS ('exosome-free serum', Life Technologies GmbH).

Infection of cells with *A. fumigatus*

A549 epithelial cells were seeded into 15 cm culture dishes at concentrations of 2×10^7 cells/dish in EV-depleted medium on the day prior to infection and incubated at 37°C and 5% (v/v) CO_2. On the day of infection, fungal conidia suspensions were washed by centrifugation with 1800 × *g* at 4°C for 5 min and the pellet was resuspended in 900 µl sterile PBS. Conidia were opsonized by the addition of 100 µl normal human serum followed by incubation at 37°C and centrifugation with 350 rpm for 30 min. Subsequently, the conidia were washed three times with sterile phosphate buffered saline (PBS) and the concentration determined using a Thoma haemocytometer. Cells were washed using PBS and fresh prewarmed EV-depleted medium in addition to opsonized fungal conidia to a multiplicity of infection of 5, was added to the cells. Control experiments were treated with medium without fungal conidia. The plates were incubated at 37°C and 5% (v/v) CO_2 for 8 or 24 h before EV isolation by size-exclusion chromatography (SEC).

EV isolation by SEC

Conditioned cell culture medium was collected from cells and centrifuged at 3000 × *g* and 4°C for 15 min, filtered through a 0.22 µm syringe filter (Carl Roth) and concentrated using Amicon Ultra-15 centrifugal filters (molecular weight cut-off: 100 kDa; Merck) by centrifugation at 4°C and 3220 × *g*. First, as a pre-experiment to test for successful isolation of EVs samples were loaded onto prewashed qEV 70 nm SEC columns (Izon). Samples were isolated using Ca^{2+}/Mg^{2+}-free PBS (Gibco). The first 2 ml of flow through corresponding to fractions 1–4 were collected followed by the collection of single fractions of 0.5 ml each until

fraction 12. All of these samples were subjected to nanoparticle tracking analysis (NTA) analysis to check for particle size and concentration in the different fractions. Finally, throughout the remaining study, concentrated samples were loaded onto pre-washed qEV 70 nm SEC columns (Izon) and isolated using Ca^{2+}/Mg^{2+}-free PBS (Gibco). Based on the results from the pre-experiment and in accordance with the manufacturer's protocol, the first 3 ml corresponding to fractions 1–6 was considered as void volume and discarded, followed by collection of the 1.5 ml EV-containing fractions 7–9. EVs were used for NTA or in case of sample preparation for proteomic analysis, western blots, or treatment of fungal hyphae, further concentrated using 10 kDa cut-off Amicon Ultra-0.5 ml filters (Merck) and stored at −20°C until usage.

NTA

Particle concentrations and size distributions of purified EV samples were assessed by NTA using a NanoSight 300 device (Malvern Instruments Ltd.). Samples were measured at ambient room temperature at a constant flow rate of 20 with the camera level set to 14 and the detection threshold to 4. For each sample, either three videos of 45 s each or five videos of 60 s each were obtained as indicated and subsequently analysed with the NTA 3.2.16 software.

Proteomic analysis of isolated EVs

EVs were isolated by SEC from conditioned medium of uninfected A549 cells and cells infected with the *A. fumigatus pyrG*$^{-}$ strain after 24 h of incubation at 37°C and 5% (v/v) CO_2 in EV-depleted medium. Preparation of protein samples from SEC-isolated EV samples, LC–MS/MS analysis, and database search and analysis were performed as described before (Rafiq et al. 2022), except for the following changes: LC–MS/MS analysis was performed on a Q Exactive Plus mass spectrometer (Thermo Fisher Scientific). Gradient elution was as follows: 0–5 min at 4% B, 30 min at 7% B, 60 min at 10% B, 100 min at 15% B, 140 min at 25% B, 180 min at 45% B, 200 min at 65% B, 210–215 min at 96% B, and 215.1–240 min at 4% B. The instrument was operated in full MS/data-dependent MS2 (Top10) mode. Precursor ions were monitored at a resolution of 140 000 FWHM (full width at half maximum). After higher-energy collisional dissociation fragmentation at 30% normalized collision energy, MS2 ions were scanned at 17 500 FWHM and a maximum injection time of 120 ms. Dynamic exclusion of precursor ions was set to 30 s. Tandem mass spectra were searched against the UniProt database of *Homo sapiens* (https://www.uniprot.org/proteomes/UP000005640; 21 March 2019) and *A. fumigatus* (https://www.uniprot.org/proteomes/UP000002530; 21 March 2019) using Proteome Discoverer (PD) 2.2 (Thermo) and the algorithms of Mascot 2.4.1 (Matrix Science), Sequest HT (version of PD2.2), and MS Amanda 2.0.

Assessment of the antifungal capacity of EVs

To assess the antifungal capacity of EVs, 1×10^4 conidia of the *A. fumigatus* AfS35/pJW103 strain (Ruf et al. 2018) were seeded into an 8-well microscopy slide (µ-Slide 8 Well Polymer Coverslip, Ibidi) in 200 µl Roswell Park Memorial Institute (RPMI) medium (Gibco) and allowed to germinate for 8 h at 37°C and 5% CO_2. EVs were isolated from uninfected or infected A549 cells after 8 h via SEC and added to the germlings followed by incubation over night at the above-mentioned conditions. On the following day fungal hyphae were stained with calcofluor white (CFW), subjected to CLSM imaging using a Zeiss LSM 780 confocal microscope, and evaluated with the Zen software (Carl Zeiss).

Generation of the plasmids encoding fusion proteins and transformation of *Escherichia coli*

DNA fragments for Gibson cloning were prepared as follows: DNA fragments were amplified from an appropriate template by polymerase chain reaction (PCR) using a primer pair (Tables S2 and S3), and PCR fragments were purified using the GeneJet PCR Purification kit (Thermo Fisher Scientific). The plasmid backbone was prepared by restriction digestion of the circular plasmid pNLF1-N (Promega) with *Eco*RV or *Eco*RI for C- or N-terminal cloning, respectively. Gibson cloning was performed using the NEBuilder HiFi DNA Assembly Master Mix (New England Biolabs) according to the manufacturer's protocol using the primers described in Table S3, and the reaction was subsequently used for the transformation of chemically competent *E. coli* cells (NEB® Turbo Competent *E. coli*, New England Biolabs). Each reporter construct is driven by a CMV promoter.

Transient transfection of A549 epithelial cells using Lipofectamine 3000®

Transfection using Lipofectamine® 3000 (Invitrogen) was performed in 24-well plates according to the manufacturer's instructions. Briefly, on the day before transfection, A549 epithelial cells were seeded into a 24-well plate at densities of 1×10^5 cells/well and incubated at 37°C and 5% (v/v) CO_2 for 20 h to allow the cells to attach. The transfection solution per well was prepared as follows: in two separate reactions, 1.5 µl Lipofectamine® and 1 µl P3000® reagent, together with 500 ng of the desired plasmid DNA for transfection, were diluted in 25 µl F12-K medium (Gibco). The contents of both tubes were combined to yield the transfection reaction, which was incubated at room temperature for 10–15 min. In the meantime, the cells were washed using prewarmed PBS and 450 µl pure F-12 K medium was added to each well. A volume of 50 µl of the transfection reaction was added to the wells in a dropwise manner, followed by gentle swirling of the plate to ensure an equal distribution. The plates were incubated at 37°C and 5% (v/v) CO_2. 22 h post-transfection, cells were washed with prewarmed PBS and incubated in 1 ml EV-depleted medium. The cells were incubated under the abovementioned conditions for the appropriate times depending on the following experiments. For microscopy, cells were seeded on glass cover slips prior to transfection. On the day of microscopy, cell membranes were stained with Cell Mask Deep Red (Invitrogen) for 10 min at 37°C and nuclei with DAPI-containing mounting medium (Roti-Mount FluorCare DAPI; Carl Roth).

Assessment of cell viability

To assess cell viability, lactate dehydrogenase (LDH) assays were performed using a commercially available fluorometric LDH assay kit (Abcam) according to the manufacturer's protocol. Briefly, culture medium was collected from transfected and nontransfected control cells after 24 h, centrifuged at 10 000 × *g* at 4°C for 5 min, and supernatants were transferred to fresh microcentrifuge tubes. Cell lysates were also prepared from untreated cells by scraping and resuspension in assay buffer to assess the maximum LDH amount required for the calculation of cell viability. Cell supernatants and lysates were kept on ice and either directly used for measurement or snap frozen and stored at −20°C until the following day. Standards and reagents were prepared freshly for every measurement. Samples and standards were

diluted in assay buffer and after addition of the assay reagent, fluorescence signal was measured in kinetic mode at 37°C at excitation/emission 535 ± 15 nm/587 ± 20 nm every 2 min for a total of 30 min using a plate reader M200 PRO plate reader (Tecan group Ltd.). Viability was calculated according to the method in the protocol.

GW4869 treatment of cells

GW4869 (Sigma Aldrich) was resuspended in dimethyl sulfoxide (DMSO) to a final concentration of 10 mM. This oversaturated stock solution was used for further dilution in cell culture media as previously described in the literature (Józefowski et al. 2010, Essandoh et al. 2015, Slivinschi et al. 2022). Transfected A549 cells were washed with PBS 22 h post-transfection and incubated in 1 ml F-12 K medium containing 1% (v/v) EV-depleted FCS and the appropriate amount of GW4869 to obtain final concentrations of 20 and 40 µM. Negative controls were incubated in culture media without the addition of GW4869 while DMSO controls were incubated in culture media containing the identical volume of DMSO as 40 µM GW4869 stock solution in the treated samples. Since DMSO is itself toxic, the highest volume of DMSO without the inhibitor was used as a control to ensure potential outcomes were not due to DMSO toxicity. Cells were incubated at 37°C and 5% (v/v) CO_2 for 6 h. All conditions were carried out as three technical replicates per biological replicate.

EV isolation using polymer-assisted precipitation

Conditioned cell culture medium was collected from transfected cells after 6 or 24 h, depending on the experiment, and centrifuged at 3000 × *g* at 4°C for 15 min to pellet dead cells and debris. For EV isolation 500 µl of the supernatants were transferred to fresh microcentrifuge tubes and the miRCURY® Exosome Cell/Urine/CSF Kit (Qiagen) was used according to the manufacturer's protocol. Briefly, 200 µl of precipitation buffer B was added to the supernatant and mixed thoroughly by vortexing. The samples were incubated at 4°C for 1 h followed by centrifugation with 10 000 × *g* at room temperature for 30 min to pellet EVs. The supernatants were completely removed by gentle pipetting and stored for NLuc measurement when required. The remaining EV pellet was resuspended in filtered PBS. Samples were used directly for NTA analysis, measurement of the NLuc signal, or snap frozen in liquid nitrogen and stored at −80°C until usage.

Western blot analysis

Cell lysates of transfected and nontransfected control cells were prepared by scraping and resuspension in radioimmunoprecipitation assay (RIPA) buffer (Thermo Fisher Scientific) supplemented with 1X protease inhibitor (Roche). EV lysates were prepared by addition of RIPA buffer and 1X protease inhibitor to isolated EVs. Protein concentrations were determined using the Qubit 4 Fluorometer with the Qubit Protein Broad Range Assay Kit (Thermo Fisher). 15 or 40 µg of protein were mixed with 1x NuPAGE LDS sample buffer (Thermo Fisher) and incubated at 95°C for 10 min. Protein preparations were loaded onto NuPAGE 4%–12% Bis Tris gels (Invitrogen) for separation followed by blotting onto a 0.2 µm pore size polyvinylidene fluoride (PVDF) membrane (Invitrogen) in an iBlot 3 western blot transfer system device (Thermo Fisher Scientific) using the preset settings for broad-range protein transfer. Membranes were blocked with 5% (w/v) milk powder in PBS with 0.5% (v/v) Tween20 for 1 h at room temperature and subsequently incubated with the respective primary antibodies diluted in 5% (w/v) milk powder in PBS with 0.5% (v/v) Tween20 at 4°C overnight. The following day, membranes were washed three times with PBS with 0.5% (v/v) Tween20 for 10 min before incubation with the secondary antibody for 1 h at room temperature. Washing steps were repeated as described above and membranes were developed by addition of 1-Step Ultra TMB Blotting Solution (Pierce, Thermo Fisher Scientific). Anti-CD9 (Abcam, AB236630), Anti-CANX (Abcam, AB22595), Anti-CD81 (Abcam, AB109201), Anti-CD63 (Abcam, AB271286 and AB134045), Anti-Lamin A (Cell Signaling Technology, 133A2), and Anti-ALIX (Cell Signaling Technology, 3A9) were used as primary antibodies. The secondary antibodies used were goat Antirabbit IgG H&L (HRP) (Abcam, AB6721) and horse Antimouse IgG (HRP) (Cell Signaling Technology, 7076S).

Lysis of EVs

Conditioned cell culture media was collected from transfected cells after 24 h and centrifuged with 3000 × *g* at 4°C for 15 min to pellet dead cells and debris. A volume of 400 µl of the supernatants were treated with 10% (v/v) Triton-X 100 at a final concentration of 0.2% (v/v) for 15 min at room temperature. During this time samples were inverted and vortexed regularly. After incubation, 300 µl of the sample was transferred to a new microcentrifuge tube for EV isolation using the miRCURY® Exosome Cell/Urine/CSF Kit (Qiagen) as described earlier.

Measurement of the NLuc activity

NLuc activity was measured from cell culture media and isolated EVs from transfected cells using the NanoGlo® Luciferase Assay System (Promega GmbH, Germany) according to the manufacturer's protocol with slight modifications. Briefly, 10 µl of sample and 15 µl of dH_2O were pipetted into the wells of a white, flat-bottom 96 well plate. The assay reagent was prepared by mixing 2 µl of NanoGlo® Luciferase Assay Substrate with 100 µl of NanoGlo® Luciferase Assay Buffer. A volume of 25 µl of the reagent was added to each well and mixed on a plate shaker. After 3 min of incubation at room temperature, the NLuc activity was examined by measurement of the luminescence signal using an Infinite M200 PRO plate reader (Tecan group Ltd.).

Imaging flow cytometry

Imaging flow cytometry of isolated EVs from transfected cells was performed using an Amnis® ImageStream^X MKII device. Briefly, cells were transfected and washed as described above. Conditioned cell culture media from 2.4 × 10^6 cells per condition and construct was collected after 24 h and EVs were isolated via polymer-assisted precipitation. Isolated EVs were resuspended in 100 µl, 0.22 µm filtered Ca^{2+}/Mg^{2+}-free PBS (Gibco) and stored at −20°C. EVs from nontransfected cells served as negative control. The device was calibrated before each use. The magnification was set to 60x, flow speed to low, and sensitivity to high. Brightfield images were obtained in channels 4 and 10, green fluorescence (488 nm) in channel 2, and the side scatter (SSC, 785 nm) in channel 6. Laser intensities were adjusted to 120 mW for the green laser and 5.16 mW for the SSC. All events including the device-internal speed beads were acquired, and the number of events was set to 20 000 per sample. Analysis of the data was performed using the Image Data Exploration and Analysis Software (IDEAS®, Amnis), version 6.2. Briefly, EVs were considered to appear as particles without a visible brightfield signal, hence the area of the brightfield signal was plotted against the intensity of the brightfield signal. This allowed us to exclude all events with a brightfield signal from the sample population and included the device-internal SpeedBeads as well as clumps of cellular material. Subsequently,

to visualize GFP-labelled EVs, the signal intensity of the GFP channel was plotted against the normalized frequency of the occurring events. Within these plots a cut-off was set at 1×10^3 for particles to be assessed as GFP-positive while particles with GFP intensity signals below this threshold were considered to be GFP-negative.

Treatment of fungal hyphae with reporter gene-expressing EVs

A. fumigatus conidia were washed by centrifugation at 1800 × *g* and 4°C for 5 min, resuspended in sterile dH_2O and the concentration was determined using a Thoma haemocytometer. 2×10^4 spores in 300 µl RPMI were pipetted into a glass bottom channel slide (µ-Slide Luer, 0.6, Glass Bottom, Ibidi) and incubated at 37°C and 5% (v/v) CO_2 for 8 h or overnight to allow for germination or the formation of hyphae, respectively. For EV treatment, 150 µl of the spent media was removed from the channel slide and isolated EVs from 2.4×10^6 transfected cells resuspended in 150 µl fresh RPMI were added to the hyphae. Due to challenges in quantifying the exact number of tagged EVs, we can only approximate the number of particles delivered to *A. fumigatus* based on our transfection efficiency and quantification of total particles by NTA. We used a ratio of roughly 250 to 1 for cells to fungus, but as we expect only 10%–15% of cells to be transfected and many EVs to be lost during isolation, we expect to have only a minor excess of EVs to fungal hyphae in the actual experiment. To achieve a more homogenous distribution of the EVs within the channel slide, 150 µl media was removed from the channel opening on the right-side and readded into the left-side opening of the channel. This step was repeated five times for every sample. Negative controls were treated similarly but with cell culture media lacking labelled EVs. Channel slides were then incubated at 37°C and 5% (v/v) CO_2 for a total of 24 h prior to being subjected to CLSM imaging using a Zeiss LSM 780 confocal microscope with a 63x oil immersion objective lens with a numerical aperture of 1.40, a refractive index of $n = 1.518$, and voxel size of 188 × 188 × 850 nm. Evaluation of the images was performed using the Zen software (Carl Zeiss). Live cell imaging was performed by addition of labelled EVs to *A. fumigatus* germlings as described above. Samples were incubated in the incubation chamber of the Zeiss LSM 780 confocal microscope at 37°C with 5% (v/v) CO_2. A preset z-stack of images was captured every 30 min using the 63x oil immersion objective lens with a numerical aperture of 1.40 and a refractive index of $n = 1.518$.

Treatment of fungal hyphae with stained EVs

1×10^4 conidia in 200 µl RPMI were seeded into the chambers of an 8-well microscopy slide (µ-Slide 8 Well Polymer Coverslip, Ibidi) and incubated at 37°C and 5% (v/v) CO_2 for 8 h to allow for germination. After the incubation time, MemGlow 560 (Cytoskeleton) was used to stain concentrated EV samples isolated from 1×10^7 nontransfected A549 cells per sample by SEC. More precisely, MemGlow 560 was added to the sample to reach a final concentration of 200 nM and the sample was directly mixed thoroughly by vortexing and immediately thereafter added into the media of the respective wells of the microscopy slide. The samples were then mixed by carefully pipetting up and down and the microscopy slide was returned to 37°C and 5% (v/v) CO_2 for 16 h. Control samples were treated with MemGlow 560 diluted in unconditioned media to a final concentration of 200 nM. The following day hyphae were stained with CFW, subjected to CLSM imaging using a Zeiss LSM 780 confocal microscope with a 63x oil immersion objective lens with a numerical aperture of 1.40, a refractive index of $n = 1.518$, and a voxel size of 132 × 132 × 400 nm. Images were evaluated with the Zen software (Carl Zeiss).

Imaging analysis

Three-dimensional images were provided in the CZI (Carl Zeiss Image) native microscopy format. The main steps of the image processing and quantification are summarized below. At first, the raw 3D images were deconvolved using the Huygens Professional software (SVI, Hilversum, The Netherlands, https://www.svi.nl), applying a measured point spread function detected from the actual samples using 170 nm fluorescent plastic beads with excitation and emission wavelengths that matched those of the biological samples. The deconvolved images were saved in TIFF format and proceeded to Imaris (Bitplane, Zürich, Switzerland, https://www.bitplane.com) for further analysis. Here, Imaris 10.2 was applied, where we used batch processing scripts to segment all components, including the hyphal wall, EVs, and the mitochondria. Each processed image was manually checked for possible segmentation errors. The hyphal segmentation revealed the actual wall boundaries, allowing the precise measurement and visualization of the EVs' spatial position relative to the hyphal cell wall. Furthermore, EVs were quantified after segmentation as Spots objects in Imaris, where they were allowed to have various radii, in order to account for the possible presence of unresolvable small EV clusters.

Statistical analysis

GraphPad Prism 10.1.0 software was used for data plotting and statistical analysis. The Student's *t*-test was used for the comparison of two groups and one-way or two-way ANOVA for the comparison of multiple groups. All bar graphs are depicted with standard deviation of the mean. Significance was defined as follows: *, $P = < .05$; **, $P = < .01$; ***, $P = < .001$; and ns, not significant.

Results

A. fumigatus-infected A549 cells secrete EVs associated with well-characterized tetraspanins

We selected an *in vitro* cellular system fulfilling two requirements, i.e. it was relevant to fungal infection and readily transfectable, to establish a toolkit for the further study of host-derived EVs. A549 lung epithelial cells met both demands, as they have a history as a cell culture infection model for *A. fumigatus* and are routinely transfected with high efficiency (Jia et al. 2023). First, we examined the secretion of EVs by A549 epithelial cells under normal culture conditions and after infection with opsonized *A. fumigatus* conidia, a condition known to elicit antifungal EVs in other systems (Shopova et al. 2020, Rafiq et al. 2022). Spontaneously released EVs from uninfected cells and *A. fumigatus* infection-derived EVs (idEVs) produced by cells challenged with conidia were isolated from conditioned cell culture media using a combination of low-speed centrifugation, ultrafiltration, and SEC. While unconditioned media prepared with EV-free FCS did not contain any measurable EV-sized particles (Fig. S1a), isolation of EVs using SEC resulted in most of the particles being released in fractions 7–9 (Fig. S1b), which were also positive for common EV markers (Fig. S1c). Transmission electron microscopy confirmed the presence of round, cup-shaped structures ranging in size from 50 to 100 nm in sample preparations from both infected and non-infected A549 cells (Fig. 1A). Next, the concentration and size of EVs and idEVs isolated at different time points were determined using NTA. We observed a significant increase in the particle

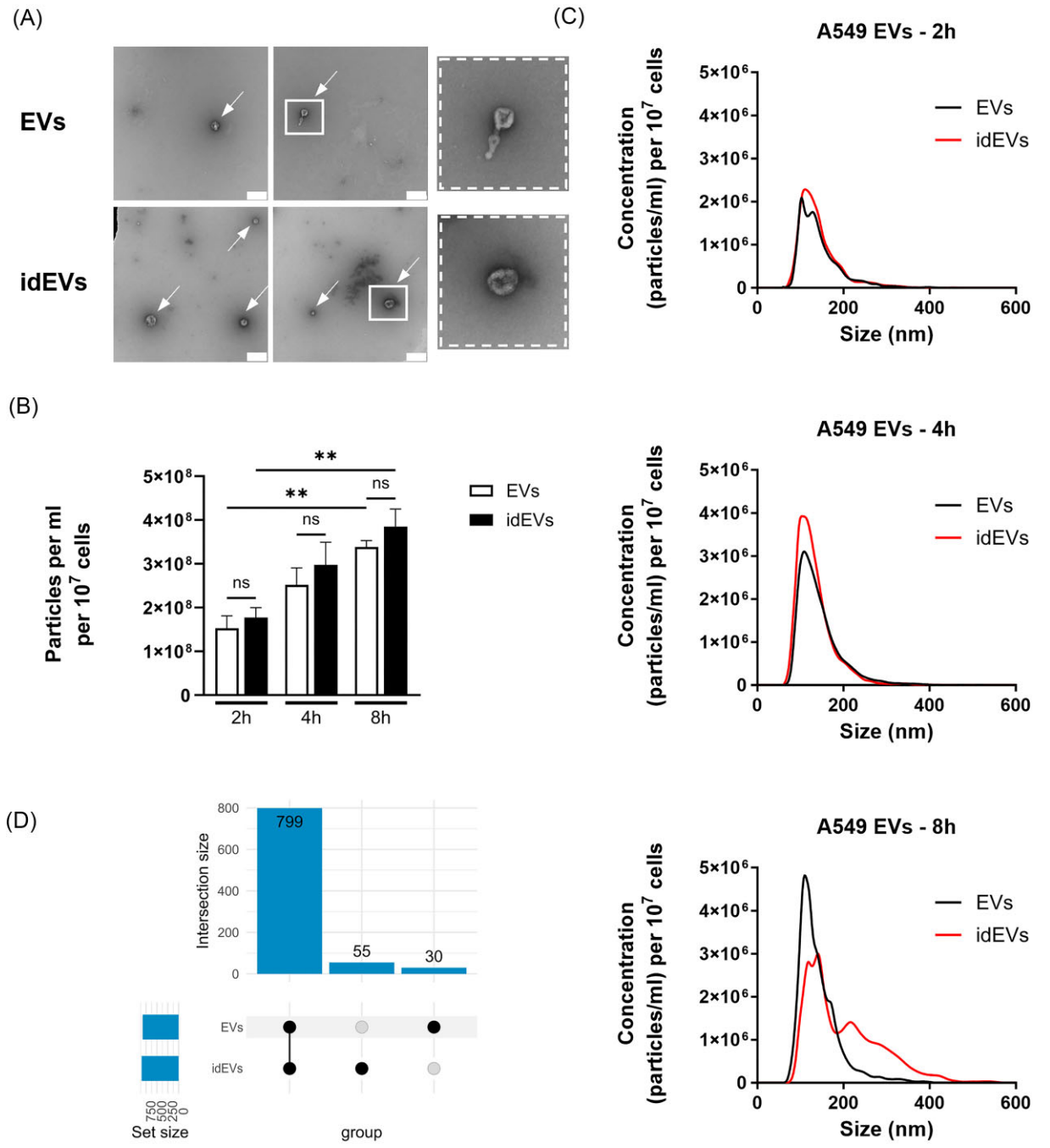

Figure 1. (A) Representative transmission electron microscopy images of A549 EVs (arrows). Upper lane: EVs were isolated from cell culture supernatants of untreated cells (spontaneously produced EVs). Lower lane: EVs were isolated from cell culture supernatants of cells previously infected with *A. fumigatus* conidia (*A. fumigatus*-induced EVs; idEVs). Scale bar: 200 nm. (B) Concentration of particles isolated from cell culture supernatants of untreated or infected A549 cells at different time points. (C) Size distribution of the isolated particles. Concentration and sizes of isolated EVs were measured using NTA. (D) Upset R plot showing the intersection of proteins detected by LC–MS/MS proteomic analysis of EVs isolated from A549 cells either left untreated (EVs) or infected with *A. fumigatus* (idEVs). Data obtained from three biological replicates. *, $P = < .05$; **, $P = < .01$; and ns, not significant.

concentration in the samples after 8 h of incubation for EVs and idEVs but no differences in the concentration between the two culture conditions (Fig. 1B). Similarly, size distributions did not greatly differ between EVs and idEVs after shorter periods of incubation and ranged between about 70–300 nm, with a peak at ~110 nm. After 8 h, NTA measurements of idEVs revealed a broader size range of isolated particles in the idEV samples with major peaks at around 120 and 140 nm, and a smaller peak at 215 nm that was not observed in the EV group, however still resides within the expected size range for EVs (van Niel et al. 2018) (Fig. 1C). Cell viability was confirmed to be unaffected by infection using LDH release assays (Fig. S1d).

EVs have gained attention with respect to their roles during infections; however, visualization of EVs is limited due to their small sizes. We previously suggested the association and apparent internalization of human primary neutrophil-derived EVs into

A. fumigatus hyphae using a lipophilic dye (Shopova et al. 2020). Here, we aimed to improve on our previous efforts by tagging several previously characterized EV marker proteins with a combination of luciferase and fluorescent protein tags. To aid in selection of suitable EV marker proteins, EVs were isolated from conditioned A549 cell culture medium after a 24-h incubation period from both infected and uninfected cells by SEC. The isolated EVs were subjected to LC–MS/MS-based proteomic analysis, revealing 884 unique proteins with 30 and 55 proteins solely found in the EV and idEV sample, respectively (Dataset S1). Principal component analysis revealed that these samples were not grossly different, but EV sample 2 was a slight outlier driven by principle component 2 at 5.54% (Fig. 1D, Fig. S2a). We did observe significant differences for a limited number of proteins (Fig. S2b), but in general the proteome of EVs appeared quite similar between the EVs and idEVs, with the most obvious changes occurring as serum proteins (e.g. IGHM, APOA1 increased in the idEVs) likely introduced by the opsonization process of *A. fumigatus* conidia prior to infection of the host cells. EVs and idEVs were both tested for their antifungal capacity using an *A. fumigatus* mitochondrial GFP reporter strain (Ruf et al. 2018) in a host cell-free system as previously described for PMNs (Shopova et al. 2020) and PLB-985 cells (Rafiq et al. 2022), in which *A. fumigatus* germlings are challenged with isolated EVs for 16 h, followed by the evaluation of the mitochondrial network integrity. In our assay, in both cases the mitochondrial network appeared largely intact and similar to the untreated growth control, suggesting that EVs isolated from naïve or *A. fumigatus*-infected A549 cells are not overtly antifungal against *A. fumigatus* (Fig. S3). This finding might not be surprising as A549 EVs lacked most of the antimicrobial proteins previously detected in PMN EVs (Shopova et al. 2020). We were able to confirm the presence of the three tetraspanins CD9, CD81, and CD63 that are generally accepted EV marker proteins. Although the nuclear lamina protein, lamin A (LMNA), was generally found in EVs from A549 cells, both EV samples were negative for the endoplasmic reticulum-associated protein calnexin (CANX), indicative of good purity of the isolated EV fractions using SEC (Welsh et al. 2024). Due to the similarity between EVs and idEVs in terms of protein content and the lack of apparent antifungal activity, the remainder of the study was performed using spontaneously released EVs to exclude potential artifacts arising from opsonins that are introduced by the opsonization of conidia during the infection process.

Transfected A549 epithelial cells properly express and localize tetraspanin-fusion proteins

After identifying appropriate EV marker proteins, we created plasmids encoding fusion proteins of one of these EV marker proteins, a NLuc, and the fluorescent protein GFP-Spark (green fluorescent protein; GFP). Despite the presence of LMNA in the EV samples as detected in our proteomic analysis, plasmids encoding for NLuc-GFP-labelled CANX and LMNA fusion proteins were generated as potential controls intended to serve as indicators of the level of introduction of cellular contaminants during EV isolation (Fig. 2A). Fusion proteins were each driven by the CMV promoter and constructed to encode an N-terminal NLuc followed by the sequence for GFP and the respective tetraspanin or LMNA at the C-terminal end to not mask the nuclear localization sequence (Anderson et al. 2021). Accordingly, since CANX has a signal peptide localized at its N-terminus (Paskevicius et al. 2023), the fusion protein was generated to encode N-terminal CANX followed by NLuc and a C-terminal GFP. Purified plasmids were used for the transient transfection of A549 alveolar epithelial cells using a liposome-based approach. Successful transfection and expression of the fusion proteins were verified after 24-h incubation by fluorescence microscopy and measurement of the luminescence signal in the cell culture supernatant (Fig. 2, Fig. S4 and S5). Generally, GFP fluorescence was detected in cells transfected with all the plasmids. LDH assays were performed on wild-type and transfected cells to test for cytotoxicity caused by the transfection itself or the specific plasmid preparations. All transfected cells showed slight decreases in viability compared to the nontransfected control cells; however, this was not influenced by the plasmid used (Fig. S5a). In addition, NTA analysis revealed no difference in particle concentration and size distribution of EVs isolated from nontransfected cells compared to transfected cells expressing the tetraspanin fusion proteins of EVs isolated using a commercially available polymer-assisted precipitation method containing polyethylene glycol (PEG) to specifically isolate EVs from the small-scale transfection experiments (Fig. S5b). To observe the subcellular localization of the fusion proteins, transfected cells were subjected to CLSM. The majority of NLuc–GFP–CD63 fusion proteins accumulated in intracellular, vesicle-like structures and to a lesser extent on the plasma membrane (Levy et al. 2020, Mathieu et al. 2021, Fan et al. 2023) (Fig. 2B, Fig. S4). NLuc–GFP–CD81 was localized within the cytoplasm partly accumulating in intracellular vesicles and partly to the plasma membrane (Eppler et al. 2011), whereas NLuc–GFP–CD9 fusion proteins were mainly localized to the plasma membrane of the cells (Mathieu et al. 2021) (Fig. 2B, Fig. S4a). For the CANX fusion proteins, fluorescent signals were diffusely distributed around the nucleus throughout the cytoplasm (Myhill et al. 2008, Jun et al. 2014), whereas the signal of the LMNA-fusion proteins were visible around the nucleus as expected (Anderson et al. 2021) (Fig. S4a). In addition, luminescence activity was detected in varying intensities in the cell culture supernatants of all transfected cells (Fig. 2C). An additional NLuc–GFP fusion protein was tried as a negative control, but this protein was nonspecifically localized throughout the whole cell, including the nucleus and extracellular space (Hall et al. 2012) (Fig. S4b). Altogether the results confirm the successful production of the fusion proteins, their expected cellular localization, and suggest no major adverse effects of genetic labelling on intracellular trafficking of the tetraspanins.

The CD9-, CD81-, and the CD63-fusion proteins are associated with EVs

In contrast to the tetraspanin fusion proteins, the CANX and LMNA fusion proteins were originally not expected to be sorted into EVs by the transfected cells or secreted into the cell culture supernatant; however, luminescence signals were detected in the supernatants for both LMNA- and to a lesser extent CANX-fusion proteins. Thus, to examine the origin of the measurable luminescence signal, PEG precipitation buffer was added to the conditioned cell culture media and incubated at 4°C followed by low-speed centrifugation, resulting in enrichment of the EVs in the pellet. We hypothesized that the tetraspanin fusion proteins associate with EVs, which in turn would result in an accumulation of the luminescence signal in the EV pellet. In contrast, as shown by our proteomic findings, the CANX and LMNA fusion proteins were expected to be underrepresented or absent in A549 EVs, therefore the signal was hypothesized to mainly accumulate in the EV-depleted supernatant of the sample after EV isolation.

Following EV isolation, NLuc activity was assessed in the resuspended EV pellets as well as in the EV-depleted supernatants.

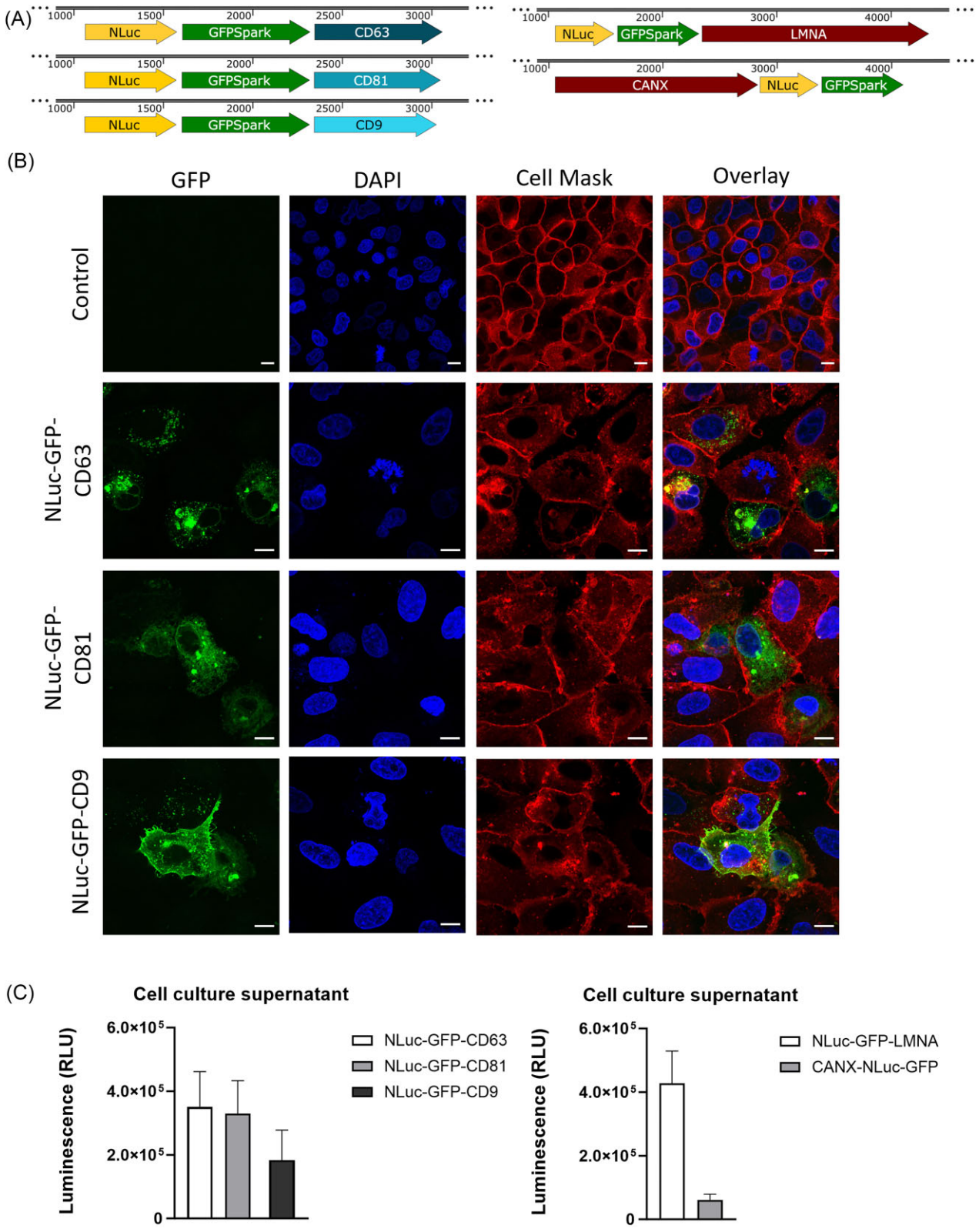

Figure 2. (A) Scheme of the fusion proteins. The tetraspanins CD63, CD81, and CD9, and LMNA were N-terminally tagged while CANX was C-terminally tagged with a NLuc and a GFPSpark (short: GFP). (B) CLSM analysis revealed the expression of the different tetraspanin fusion proteins within transfected A549 epithelial cells based on the GFP signal. Nontransfected cells imaged with the same settings for GFP showed no background signal or autofluorescence. Nuclei of the cells were stained with DAPI and the cell membrane was stained using Cell Mask Deep Red. Scale bar: 10 µm. (C) Measurement of the luminescence signal in the cell culture supernatant of transfected cells. Positive signals were obtained for cells transfected with either of the plasmids encoding the tetraspanin as well as control fusion proteins. Results were obtained from at least four biological replicates.

EV isolation using this method resulted in a high luminescence signal deriving from the resuspended EV pellets compared to the EV-depleted supernatants of cells expressing the CD63 and CD9 fusion proteins, indicative of the fusion proteins being associated with EVs (Fig. 3A). In the case of the CD81-fusion proteins the enrichment of the signal in the EV fraction was not as prominent and a comparably high signal was also derived from the supposedly EV-depleted supernatant. As expected, little NLuc activity was detected in the EV pellets of cells expressing the CANX and LMNA fusion proteins, but high signals were measurable in the EV-depleted supernatants, suggesting that the respective protein fusions were not associated with EVs.

To further confirm the association of the labelled tetraspanins with EVs, conditioned cell culture media were treated with the nondenaturing detergent Triton X-100 prior to EV isolation. Addition of Triton X-100 leads to the lysis of EVs in the sample (Fig. S5c), releasing EV-associated proteins and molecules into the media and preventing their subsequent precipitation during polymer-assisted EV isolation. Thus, assuming the association of the labelled tetraspanins with EVs, in this setting successful lysis of the EV membrane will result in the luminescence signal deriving from the EV-depleted supernatants instead of the pellets as seen before. Indeed, Triton X-100 treatment led to a clear shift of the luminescence signal from the EV pellet to the EV-depleted supernatant for samples of cells expressing either of the labelled tetraspanins (Fig. 3B). This finding further strengthened our hypothesis that these fusion proteins are associated with EVs.

Lastly, transfected cells were treated with the neutral sphingomyelinase inhibitor GW4869 prior to collection of conditioned cell culture media. GW4869 is known to partially block exosome biogenesis (Trajkovic et al. 2008, Willms et al. 2016, Catalano et al. 2020). Assuming that the tetraspanin fusion proteins are associated with EVs, treatment of transfected cells with the inhibitor was expected to decrease the EV-derived luminescence signal in our assays. Cell culture supernatants were collected 6 h post-treatment either with the inhibitor or DMSO as a control and subjected to EV isolation by polymer-assisted precipitation. Subsequently, the resulting EV-enriched pellets were resuspended, and the NLuc signal measured (Fig. 3C). Due to high variability of the luminescence signal values between different biological replicates, values were normalized to the untreated controls. Indeed, cell culture media obtained from cells treated with GW4869 revealed a significantly decreased NLuc signal in the EV-pellet (Fig. 3C). The decrease in measurable signal correlated positively with increasing concentrations of the inhibitor. In contrast, cells treated with DMSO did not exhibit significantly different NLuc signals compared to the nontreated controls, indicating that the effect is not correlated to DMSO-induced cell toxicity. In addition, LDH assays were performed to verify that the dose-dependent decrease in EV release is not caused by cell death due to the inhibitor itself. A significant decrease of viability was only seen for cells expressing the CD63-fusion proteins when treated with 20 µM GW4869 (Fig. S5d). Thus, the LDH assay indicates that cell death is not solely responsible for the significantly reduced NLuc signal in EV-pellets from transfected cells and supports our previous findings that the fusion proteins are associated with EVs.

Collectively, these results suggest that first, the tetraspanin fusion proteins are associated with EVs of A549 epithelial cells, and second, that transfected A549 cells can be used as reporters for the detection and quantification of secreted EVs after their isolation by measurement of luminescence signal.

GFP-labelled EVs can be visualized using imaging flow cytometry and CLSM

We next wanted to assess whether the isolated EVs from cells expressing the GFP fusion proteins can be visualized. We subjected isolated EVs from transfected and nontransfected cells to imaging flow cytometry. All events that exhibited either a brightfield, side scatter, or GFP signal were captured, including the device internal beads that are important for adjusting the focus. Measurement of the samples revealed a distinct population of events that was only detected in samples expressing the tetraspanin fusion proteins and mostly absent in the sample isolated from nontransfected control cells (Fig. S5e). Further investigation of this population revealed a high abundance of particles with no brightfield or side scatter signal but a visible GFP signal, likely corresponding to single EVs.

Next, to visualize EVs using CLSM, we set up a cell-free system in which EVs isolated from transfected cells were added to *A. fumigatus* germlings. The fungus was cultivated in RPMI in glass-bottom microscopy channel slides that offer limited space for vertical growth and instead force horizontal, planar growth of the hyphae. EV pellets resuspended in small volumes of culture media were added to the fungus and coincubated for 16 h in a humidified incubator. After the coincubation time, samples were directly observed by CLSM. To increase the contrast and resolution, we used the *A. fumigatus* strain AfS150 (Lother et al. 2014), a genetically modified strain expressing the fluorescent protein dTomato within its cytoplasm. Using this strain, overlapping of emission signals was limited and additional washing steps required for most staining protocols that could lead to the loss of EVs were eliminated. CLSM revealed visible green-fluorescent signals in samples treated with EVs isolated from transfected cells expressing any of the labelled tetraspanins compared to untreated control samples (Fig. 4). The visible signal derived from small dot-like to roundish structures, most of which appeared to consist of clusters of EVs. These clusters exhibited varying intensities and sizes with most being far below or around 1000 nm based on the green fluorescence signal, similar to the findings of other groups (Levy et al. 2020). Our NTA data of A549 EVs isolated *via* polymer-assisted precipitation with sizes of A549 EVs ranging from ∼70 to 450 nm (Fig. S5b) supports our hypothesis that the visible signals partly derive from clumps of EVs. In all cases, labelled EVs were found to colocalize with the fungus, indicating that A549 EVs are indeed able to attach to or associate with *A. fumigatus* hyphae and confirming the value of our system in tracking these interactions.

To further verify our findings, we also applied EVs isolated from nontransfected, wild-type A549 cells. To visualize these EVs, we used a novel fluorogenic membrane dye called MemGlow 560 that exhibits minimal fluorescence in its free form. Only the integration into a lipid bilayer leads to high fluorescence signals, which harbours the advantage that isolated EVs can be stained without the need for subsequent washing steps. Since the dye exhibited red fluorescence when integrated into membranes, stained EVs were added to the genetically modified *A. fumigatus* strain AfS35 pJW103 expressing a green-fluorescent mitochondrial tag (Ruf et al. 2018) that was also used to assess the antifungal capacity. Conidia were seeded in 8-well microscopy slides and allowed to germinate for 8 h prior to addition of the EVs. EVs in turn were isolated from cell culture supernatants of A549 cells *via* SEC, concentrated, and subsequently stained and added to the germlings. After 16 h of coincubation, hyphal cell walls were visualized using CFW and the samples were subjected to CLSM. Negative control

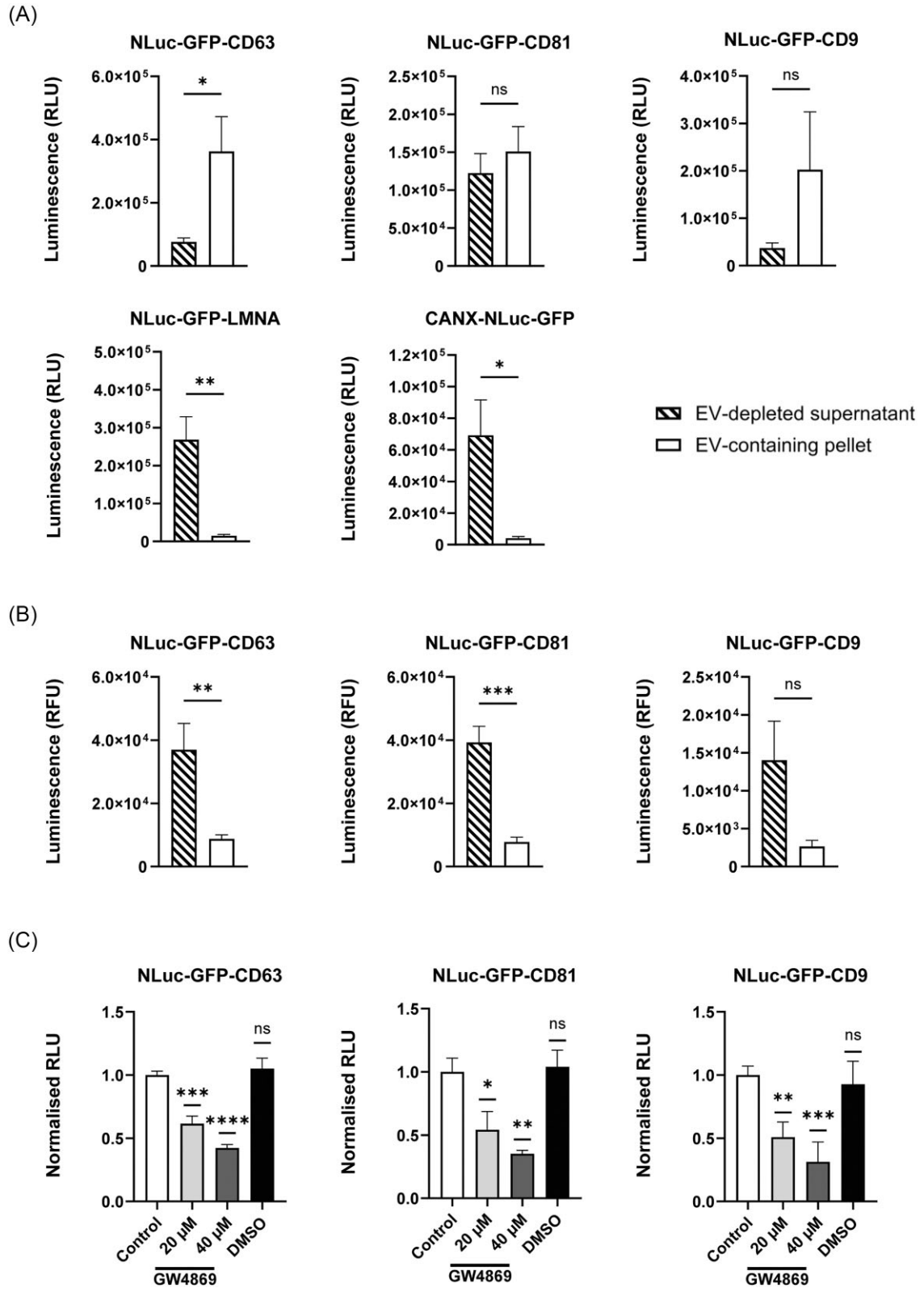

Figure 3. (A) Measurement of the luminescence signal in the EV-depleted supernatant compared to the EV-enriched pellet after EV isolation from transfected A549 epithelial cells using a polymer-precipitation-based method. EV isolation led to an increased luminescence signal deriving from the EV-containing pellet compared to the EV-depleted supernatant in cases of cells expressing the tetraspanin fusion proteins. EV isolation from cell culture media of cells expressing the LMNA and CANX control fusion proteins resulted in most of the signal deriving from the EV-depleted supernatant. (B) Measurement of the luminescence signal in the EV-depleted supernatant and EV-containing pellet of A549 EVs treated with Triton X-100 prior to EV isolation. Lysis of EVs resulted in a shift of the luminescence signal from the pellet to the supernatant. (C) Measurement of the luminescence signal in the EV-containing pellet after EV isolation from transfected A549 cells treated with GW4869 or DMSO as a control. Treatment of cells with GW4869 resulted in a dose-dependent decrease of the luminescence signal in the pellet. Results of isolated and lysed EVs were obtained from at least four biological replicates. Inhibitor assays using GW4869 were performed as three biological replicates *, $P = < .05$; **, $P = < .01$; ***, $P = < .001$, ****, and $P = < .0001$; ns, not significant.

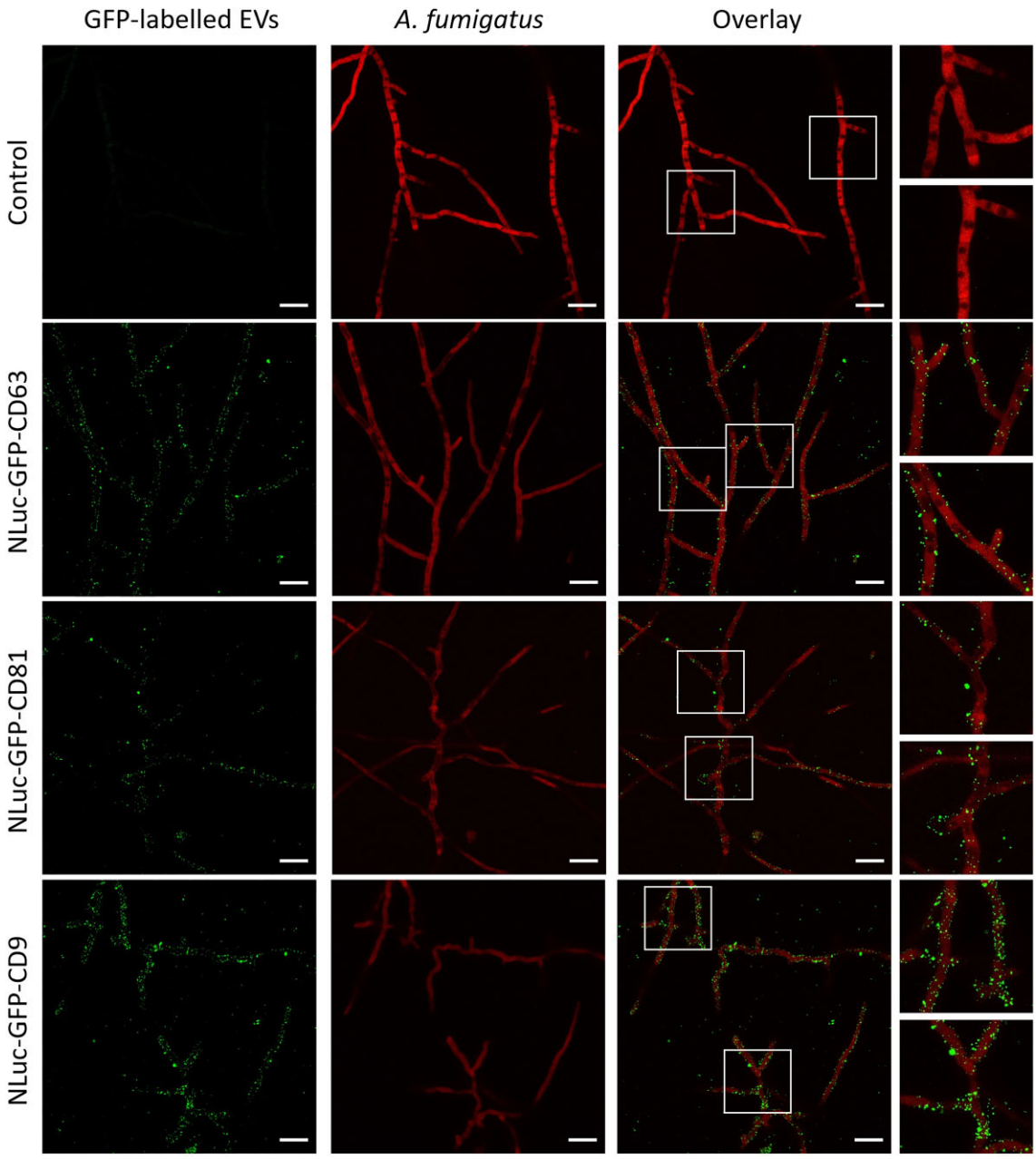

Figure 4. CLSM images revealing that labelled A549 EVs can be visualized and are able to associate with *A. fumigatus* hyphae. Resuspended EVs isolated from transfected cells expressing the NLuc–GFP-labelled tetraspanins were added to 7 h-old *A. fumigatus* dTomato germlings in a host cell-free system and incubated overnight. EVs appeared as dots with varying sizes. *A. fumigatus* treated with EVs isolated from nontransfected cells were used a control. Images were taken using a Zeiss LSM 780 confocal microscope. Scale bar: 20 µm. Representative images from >3 biological replicates per construct.

samples of hyphae treated with the dye diluted in non-EV containing medium displayed no or only minimal red fluorescence signal, showing that the dye is not able to penetrate the fungal cell wall and therefore does not stain the hyphal membrane. In samples treated with stained EVs, several dots of red fluorescence in varying size and intensity accumulating at fungal hyphae were visible (Fig. 5). In general, based on the sizes of the red fluorescence signal, EVs stained with the membrane dye appeared to be smaller in size than the genetically labelled EVs, potentially due to reduced clumping and cluster formation after isolation using SEC.

The CLSM images were subsequently subjected to imaging analysis and 3D reconstruction to further investigate the localization of EVs regarding *A. fumigatus* hyphae (Fig. 6 and Fig. S6). Since labelled EVs were added to the *A. fumigatus* strain AfS150 expressing a cytoplasmic dTomato protein, our 3D models depict the limiting boundaries of the cytoplasm, equivalent to the hyphal membrane. Reconstruction of the EV signal revealed the association of labelled EVs with the hyphal membrane and their internalization into the hyphal lumen (Fig. 6A and B; Video S1). In the case of MemGlow-stained EVs, experiments were performed using the CFW-stained *A. fumigatus* AfS35 pJW103 strain, with the hyphal cell wall depicted in blue (Fig. 6C). Most of the MemGlow signal was localized within the hyphae. Interestingly, the signal appeared to accumulate as a tube-like structure underneath the cell wall, which became even more obvious upon reconstruction of the signal from the GFP-labelled mitochondria

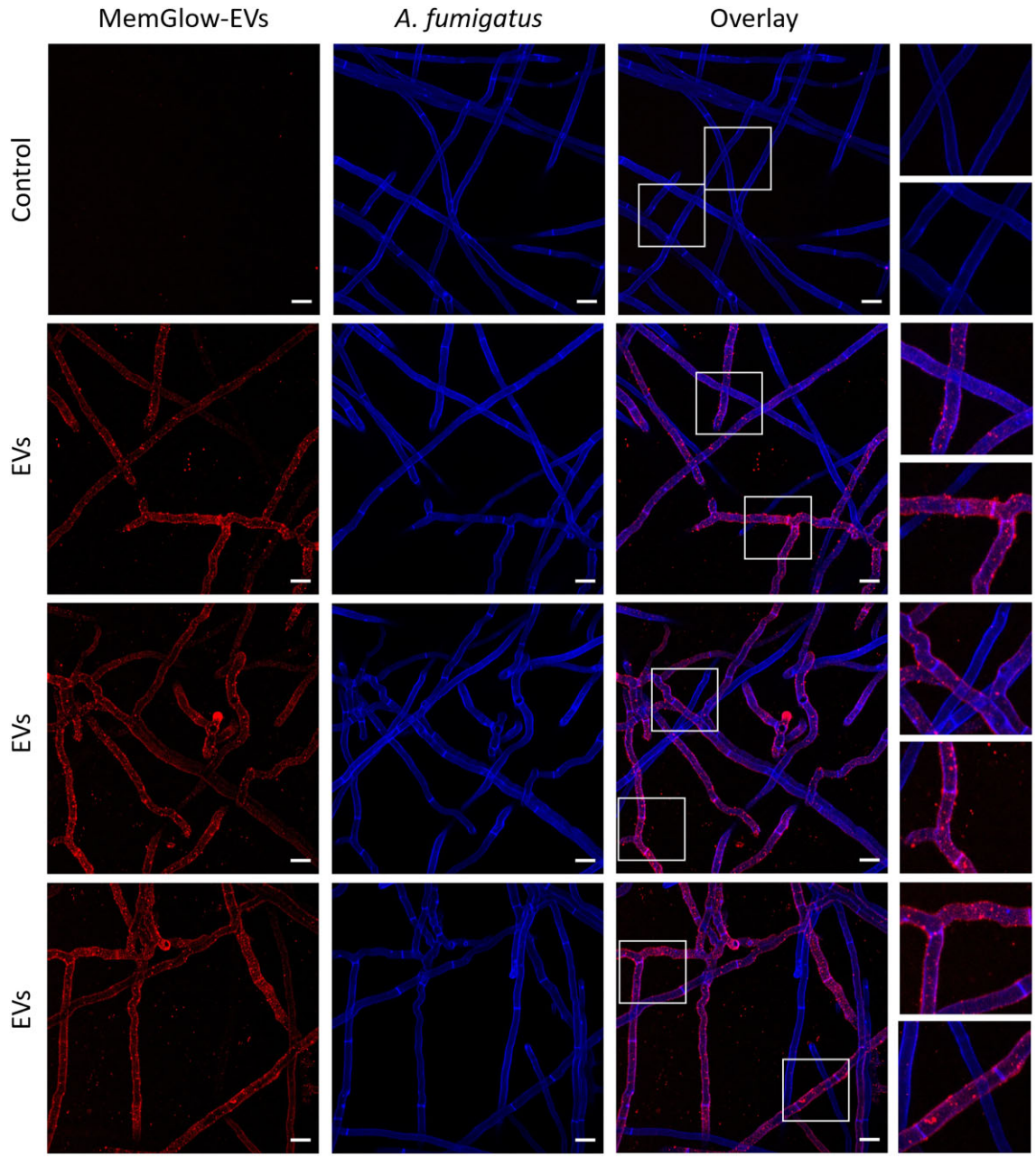

Figure 5. Representative CLSM images of stained EVs colocalizing with the *A. fumigatus* strain AfS35. EVs were isolated from nontransfected cells using size exclusion chromatography and stained with MemGlow 560 prior to addition to 7 h-old *A. fumigatus* germlings in a host cell-free system. After overnight incubation, hyphal cell walls were stained with CFW and subjected to CLSM. EVs appeared as dot-like signals with varying sizes. Control hyphae treated with MemGlow 560 in PBS exhibit no staining. Images were taken using a Zeiss LSM 780 confocal microscope. Scale bar: 20 µm. Representative images from three biological replicates.

within the hyphal lumen. These finding indicate an accumulation of the signal within or associated with the hyphal membrane, consistent with what was observed using the genetically labelled EVs.

Finally, we wanted to test whether the genetically labelled EVs can be used to track EVs in our experimental set-up using live cell imaging. As a proof-of-concept we tested EVs isolated from NLuc–GFP–CD9 expressing cells using polymer-assisted precipitation. Western blots confirmed the presence of CD9 in EVs isolated from cells expressing either of the labelled tetraspanins or nontransfected control cells. In addition, a clear band corresponding to the NLuc–GFP–CD9 fusion protein was visible for EVs isolated from cells that were transfected with the respective plasmid (Fig. S5f). Isolated EVs were then added to 8-h-old germlings of the *A. fumigatus* strain AfS150 and imaging was performed over night with a z-stack image being taken every 30 min (Videos S2–S7). In the beginning, EVs appeared as small green fluorescent dots that over time started to accumulate at the growing hyphae. Once attached, these EVs still displayed some mobility, but remained attached to the hyphae.

Discussion

PMN-derived EVs were previously found to display antibacterial (Timár et al. 2013, Lőrincz Á et al. 2015) and antifungal

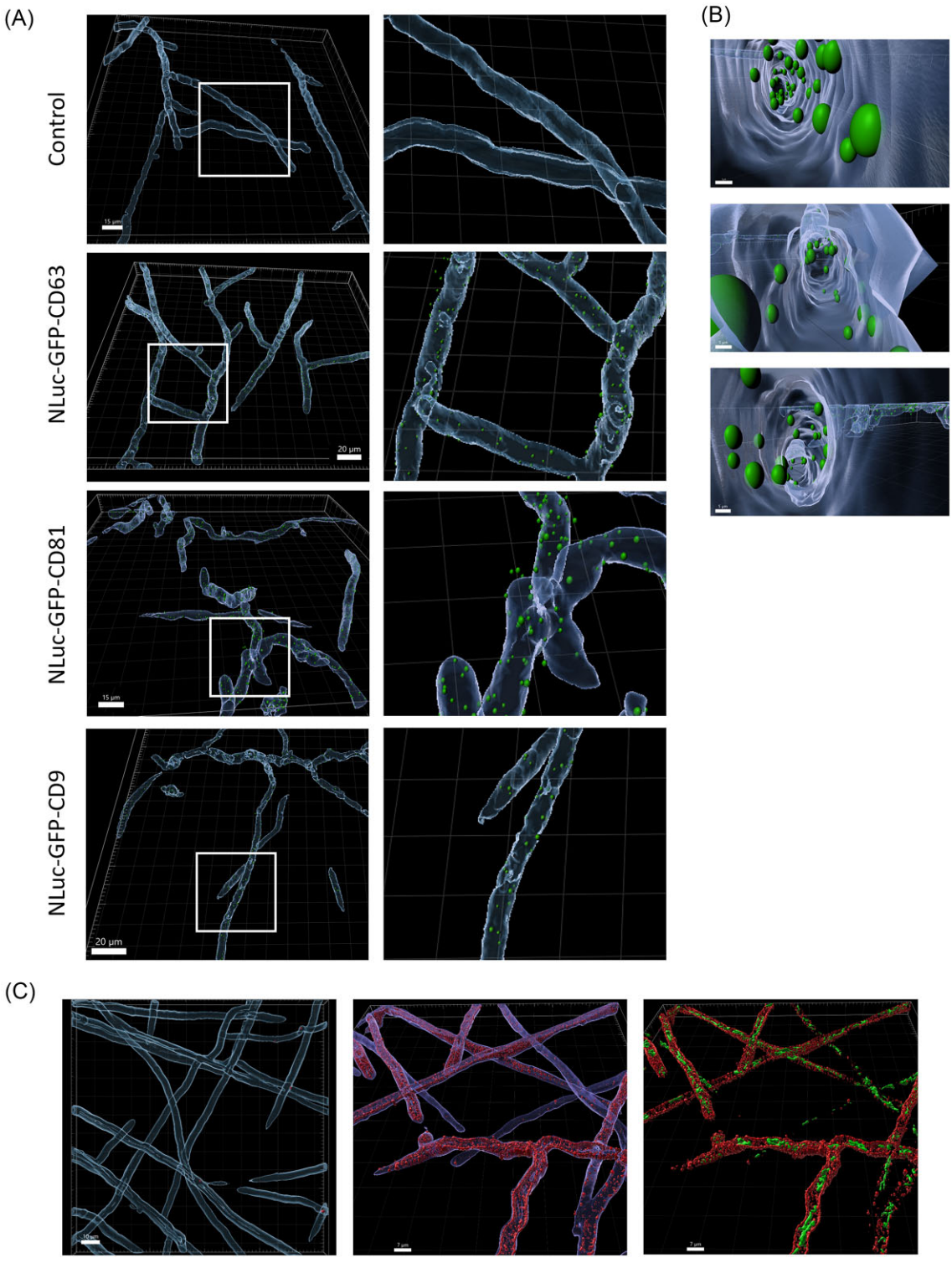

Figure 6. (A) 3D reconstruction of *A. fumigatus* hyphae CLSM images reveals the association of labelled EVs depicted as dots within hyphae. Since the *A. fumigatus* AfS150/pSK537 strain expressing a cytoplasmic dTomato protein was used here, the outer signal is equivalent with the limiting border of the hyphal lumen and thus the hyphal membrane. (B) Magnification of the 3D reconstructed hyphae confirms the association and partly internalization of NLuc–GFP–tetraspanin-labelled EVs into the hyphal lumen of *A. fumigatus*. (C) MemGlow stained EVs (red, center and right panels) accumulate within *A. fumigatus* hyphae as a tube-like structure underneath the cell wall (blue, left and center panels), likely accumulating at the hyphal cell membrane. The finding is supported by the reconstruction of the GFP-tagged mitochondria and EVs (right panel).

activities (Shopova et al. 2020, Rafiq et al. 2022) under specific conditions. Here, we attempt to investigate the first steps in the mechanism by which host EVs exert their antifungal functions by exploring the interaction between host cell-derived EVs and *A. fumigatus* hyphae. Our main goal was the visualization and tracking of these EVs in a live-cell setting; however, EVs are difficult to visualize based on their small size (<1 µm) and heterogeneity. Various methods have been employed in the past such as electron microscopy, staining with dyes, immunofluorescence, and genetic labelling of abundant EV cargo molecules, each with their own advantages and disadvantages (Chuo et al. 2018, Verweij et al. 2021). In this study, we used two different approaches, lipophilic dyes to stain EV membranes and genetic labelling of abundant EV proteins, which allowed us to detect, visualize, and track genetically labelled EVs in association with *A. fumigatus* hyphae.

A549 alveolar epithelial cells served as a tractable model as they are easy to transfect compared to immune cells and have been well-studied during infection with *A. fumigatus* conidia (Paris et al. 1997, Zhang et al. 2005, 2020, Amin et al. 2014, Jia et al. 2014, 2023). We confirmed the successful isolation of EVs and little induction of cell death by LDH release assay consistent with the literature, followed by analysis of their proteomic cargo and antifungal capacity. Interestingly, and in contrast to PMN idEVs (Shopova et al. 2020) and PLB-985 idEVs (Rafiq et al. 2022), none of the EV populations isolated exhibited antifungal activity in our host cell-free system based on an *A. fumigatus* mitochondrial integrity reporter strain. Consistently, analysis of the proteomic cargo confirmed the absence of any obvious antimicrobial proteins, opposite that of PMN idEVs (Shopova et al. 2020). Although the literature reports both activation and repression of inflammatory phenotypes in A549 cells upon coincubation with *A. fumigatus* conidia (Paris et al. 1997, Zhang et al. 2005, Amin et al. 2014, Jia et al. 2014, 2023, Escobar et al. 2016, 2018), the auxotrophic *A. fumigatus pyrG*-deficient strain used here appeared to result in a limited proinflammatory response and may contribute to our observations. This strain provides a fungal stimulus to the cells, while allowing for collection of larger amounts of EVs necessary for proteomics over longer coincubations. It remains a potential complication of these experiments that longer infection time points may result in increased cell stress, low level cell death, and/or alterations to the proteomic cargo of EVs. Fungal proteins were detected inconsistently in the proteomic samples and likely derive from coisolation of fungal proteins during EV isolation as 'contaminants' (Shopova et al. 2020, Rafiq et al. 2022).

Proteomic analysis of EVs confirmed several commonly associated proteins, including the tetraspanins CD63, CD9, and CD81, which are routinely used as EV marker proteins (Lötvall et al. 2014, Kowal et al. 2016, Lischnig et al. 2022, Tognoli et al. 2023) and to label EVs (Hikita et al. 2018, Cashikar et al. 2019, Görgens et al. 2019, Gupta et al. 2020). CANX and LMNA were included as negative controls to assess EV purity and the association of the fusion proteins with EVs (Tognoli et al. 2023). According to the minimal information for studies of extracellular vesicles (MISEV) guidelines, these proteins are typically absent or underrepresented in EVs; however, they are found in some subtypes of EVs (Théry et al. 2018, Welsh et al. 2024). Proteomic analysis of wild-type A549 cells indicated that CANX was indeed absent; however, LMNA could be detected in our EV samples. Nonetheless, we created reporters for both control markers and the tetraspanin proteins to have a full repertoire of options for expansion into multiple cell systems in the future. Successful transient overexpression of the panel of NLuc–GFP fusion proteins in A549 cells was confirmed by green fluorescence and luminescence signals in the cell culture media from transfected cells, including those encoding the CANX and LMNA fusion proteins. It is worth noting that overexpression of tetraspanins can impact EV biogenesis and cargo loading, a caveat that must always be considered with any reporter (Strohmeier et al. 2021), and subsequently future studies will be required to more finely localize our new reporters in particular EV subpopulations. Nonetheless, we observed release of all the fusion proteins into the cell culture supernatant in accordance with previous observations (Cashikar et al. 2019, Gupta et al. 2020); however, isolation of EVs from cell culture supernatants revealed that the CANX and LMNA fusion proteins were not associated with the EV fraction, as initially expected. In addition, lysis of EVs in cell culture supernatants prior to their isolation demonstrated the association of the fusion proteins with A549 EVs. As an orthogonal approach, we confirmed a dose-dependent decrease of signal in the EV-containing fraction upon treatment of transfected cells with the neutral sphingomyelinase inhibitor GW4869 known to reduce EV biogenesis via the ESCRT-independent exosome biogenesis pathway (Trajkovic et al. 2008, Kulshreshtha et al. 2013, Essandoh et al. 2015). We used high levels of GW4869 as described in the literature and did observe some LDH release indicative of cell death in this assay, yet overall the result appears to imply that the reporters decreased along with EV numbers. The successful generation of the reporter panel allowed for detection and relative quantification of EVs by luminescence signal, while simultaneously enabling their visualization within the cells for subcellular localization and transfection efficiency, simplifying the overall workflow associated with such a reporter assay.

Imaging flow cytometry on the tetraspanin reporters from isolated EVs detected events of green fluorescent particles with minimal to no visible brightfield or side scatter signal. The absence of the brightfield signal is indicative of particles with sizes below the optical resolution limit of the device of 200 nm, consistent with sizes corresponding to small EVs (Headland et al. 2014, Abels et al. 2016) and in accordance with previous studies investigating GFP-labelled EVs from THP-1 monocytes (Görgens et al. 2019) and HEK293 cells (Jurgielewicz et al. 2020), as well as immunolabelled EVs (Ricklefs et al. 2019). Using CLSM, EVs appeared as small, green fluorescent dots of varying size and intensity similar to the findings of previous studies using genetically labelled fluorescent EVs (Corso et al. 2019) and immunolabelled or stained EVs (Mondal et al. 2019). Importantly, part of the visible signal was clearly associated with fungal hyphae, indicating that A549 EVs can interact with *A. fumigatus*. This colocalization was seen for all EVs regardless of the labelled tetraspanin expressed, hinting towards a nonspecific interaction. We verified these findings using MemGlow stained A549 EVs from nontransfected cells. While the dye alone was almost completely unable to penetrate the cell wall of *A. fumigatus* hyphae, addition of stained EVs led to accumulation of colocalized signal with *A. fumigatus* hyphae as dot-like structures, similar to the EVs labelled with reporter proteins. One major difference observed between the two experiments was the amount of EVs binding to the hyphae, which is likely caused by the higher proportion of labelled EVs using the MemGlow approach. These EVs were isolated via SEC from a large number of cells. Even though this isolation method led to a dilution of the sample (Welsh et al. 2024), the total amount of labelled EVs in the final sample was likely higher than from the low-efficiency transfection experiments. While the lipophilic dye can stain many subsets of EVs, it was previously shown that the tetraspanins CD63, CD81, and CD9 distribute heterogeneously across EV subsets (Ricklefs et al. 2019, Han et al. 2021), resulting in even fewer labelled versus stained EVs. Different tagging approaches can alter the properties

and fate of EVs, so it is recommended to use different labelling methods when studying EVs (Loconte et al. 2023). Here, the similar outcomes of the two strategies employed provides confirmatory evidence for the use of either our tetraspanin fusion proteins or MemGlow dye as the situation necessitates, but certainly orthogonal support is required for each specific experiment.

Lastly, imaging analysis and 3D-reconstruction of the microscopy images indicated that both labelled and stained A549 EVs are attached and partly internalized by *A. fumigatus* hyphae. This was an interesting finding that brings us one step further into understanding how EVs can exert effects on the fungus. First, it is now clear that the interaction of EVs with fungal hyphae is not limited to EVs produced by infected cells, but instead a more widespread phenomena, potentially even serving as a food source for the fungus in some cases. It is also likely that the interaction of EVs alone cannot explain the antifungal activity previously observed for PMN (Shopova et al. 2020) and PLB-985 idEVs (Rafiq et al. 2022). The mechanisms behind the attachment of EVs to hyphae and their subsequent internalization remain unclear and will be objectives of future studies, but based on their ability to fuse with membranes (Morandi et al. 2022), one hypothesis could be that EVs are able to pass the cell wall, either actively or passively, followed by fusion of the EV membrane with the hyphal membrane to release cargo. A more active form of fungal cell-induced endocytosis also remains possible. In mammalian cells, evidence suggests that EVs can be taken up into the endosomal/lysosomal pathway via endocytosis and that the release of EV cargo within recipient cells is often pH-dependent (Mulcahy et al. 2014, Bonsergent et al. 2021). More generally, successful uptake and cargo delivery of host cell EVs by fungi was previously demonstrated in plant–fungal interactions (Cai et al. 2018, Wang et al. 2024).

In conclusion, our knowledge of host cell-derived EVs in immunity to *A. fumigatus* is still very limited. With these findings, we can confirm that EVs produced by naive human alveolar epithelial cells robustly interact with *A. fumigatus* hyphae, but fail to trigger an antifungal response. In the future, this methodological proof-of-principle using genetic labelling of A549 cell-derived EVs will serve as a platform to be expanded to other cell types as well as other target proteins.

Acknowledgements

We thank Johannes Wagener for providing the *A. fumigatus* mitochondrial-GFP strain and Maximilian Knott for excellent technical support.

Supplementary data

Supplementary data is available at *FEMSML Journal* online.

Conflict of interest: None declared.

Funding

This work was supported by the Deutsche Forschungsgemeinschaft (DFG)-funded Collaborative Research Center/Transregio 124 FungiNet (project number 210879364, projects A1, B4 and Z2), the Cluster of Excellence *Balance of the Microverse* under Germany's Excellence Strategy (EXC 2051; project ID 390713860), and the DFG-funded Collaborative Research Centre PolyTarget (Project-ID: 316213987–SFB 1278; project Z01). M.G.B. was supported by the Federal Ministry for Education and Research (BMBF: https://www.bmbf.de/), Germany, Project FKZ 01K12012 'RFIN—RNA-Biologie von Pilzinfektionen'. The funders had no role in the study design, data collection and analysis, decision to publish, or preparation of the manuscript.

Data availability

The mass spectrometry proteomics data have been deposited to the ProteomeXchange Consortium via the PRIDE (Perez-Riverol et al. 2022) partner repository with the dataset identifier PXD050398.

References

Abels ER, Breakefield XO. Introduction to extracellular vesicles: biogenesis, RNA cargo selection, content, release, and uptake. *Cell Mol Neurobiol* 2016;**36**:301–12.

Amin S, Thywissen A, Heinekamp T *et al.* Melanin dependent survival of *Apergillus fumigatus* conidia in lung epithelial cells. *Int J Med Microbiol* 2014;**304**:626–36.

Anderson CL, Langer ER, Routes TC *et al.* Most myopathic lamin variants aggregate: a functional genomics approach for assessing variants of uncertain significance. *NPJ Genom Med* 2021;**6**:103.

Bonsergent E, Grisard E, Buchrieser J *et al.* Quantitative characterization of extracellular vesicle uptake and content delivery within mammalian cells. *Nat Commun* 2021;**12**:1864.

Brakhage AA. Systemic fungal infections caused by *Aspergillus* species: epidemiology, infection process and virulence determinants. *CDT* 2005;**6**:875–86.

Brakhage AA, Zimmermann AK, Rivieccio F *et al.* Host-derived extracellular vesicles for antimicrobial defense. *Microlife* 2021;**2**:uqab003.

Cai Q, Qiao L, Wang M *et al.* Plants send small RNAs in extracellular vesicles to fungal pathogen to silence virulence genes. 2018;**360**:1126–9.

Cashikar AG, Hanson PI. A cell-based assay for CD63-containing extracellular vesicles. *PLoS One* 2019;**14**:e0220007.

Catalano M, O'Driscoll L. Inhibiting extracellular vesicles formation and release: a review of EV inhibitors. *J Extracell Vesicle* 2020;**9**:1703244.

Chuo S, Ting-Yu J, Chien C-Y *et al.* Imaging extracellular vesicles: current and emerging methods. *J Biomed Sci* 2018;**25**:91.

Corso G, Heusermann W, Trojer D *et al.* Systematic characterization of extracellular vesicle sorting domains and quantification at the single molecule—single vesicle level by fluorescence correlation spectroscopy and single particle imaging. *J Extracell Vesicle* 2019;**8**:1663043.

Denning DW. Global incidence and mortality of severe fungal disease. *Lancet Infect Dis* 2024;**24**:e428–38.

Eppler F, Semmling V, Schild C *et al.* CD81 is essential for the formation of membrane protrusions and regulates Rac1-activation in adhesion-dependent immune cell migration. *Blood* 2011;**118**:1818–27.

Escobar N, Ordonez SR, Wösten HA *et al.* Hide, keep quiet, and keep low: properties that make *Aspergillus fumigatus* a successful lung pathogen. *Front Microbiol* 2016;**7**:438.

Escobar N, Valdes ID, Keizer EM *et al.* Expression profile analysis reveals that *Aspergillus fumigatus* but not *Aspergillus niger* makes type II epithelial lung cells less immunological alert. *BMC Genomics* 2018;**19**:534.

Essandoh K, Yang L, Wang X *et al.* Blockade of exosome generation with GW4869 dampens the sepsis-induced inflammation and cardiac dysfunction. *Biochim Biophys Acta Mol Basis Dis* 2015;**1852**:2362–71.

Ewald J, Rivieccio F, Radosa L *et al.* Dynamic optimization reveals alveolar epithelial cells as key mediators of host defense in invasive aspergillosis. *PLoS Comput Biol* 2021;**17**: e1009645.

Fan Y, Pionneau C, Cocozza F *et al.* Differential proteomics argues against a general role for CD9, CD81 or CD63 in the sorting of proteins into extracellular vesicles. *J Extracell Vesicle* 2023;**12**:12352.

Görgens A, Bremer M, Ferrer-Tur R *et al.* Optimisation of imaging flow cytometry for the analysis of single extracellular vesicles by using fluorescence-tagged vesicles as biological reference material. *J Extracell Vesicle* 2019;**8**:1587567.

Gupta D, Liang X, Pavlova S *et al.* Quantification of extracellular vesicles in vitro and in vivo using sensitive bioluminescence imaging. *J Extracell Vesicle* 2020;**9**:1800222.

Hall MP, Unch J, Binkowski BF *et al.* Engineered luciferase reporter from a deep sea shrimp utilizing a novel imidazopyrazinone substrate. *ACS Chem Biol* 2012;**7**:1848–57.

Han C, Kang H, Yi J *et al.* Single-vesicle imaging and co-localization analysis for tetraspanin profiling of individual extracellular vesicles. *J Extracell Vesicle* 2021;**10**:e12047.

Headland SE, Jones HR, D'Sa ASV *et al.* Cutting-edge analysis of extracellular microparticles using ImageStreamX imaging flow cytometry. *Sci Rep* 2014;**4**:5237.

Heinekamp T, Schmidt H, Lapp K *et al.* Interference of *Aspergillus fumigatus* with the immune response. *Semin Immunopathol* 2015;**37**:141–52.

Hikita T, Miyata M, Watanabe R *et al.* Sensitive and rapid quantification of exosomes by fusing luciferase to exosome marker proteins. *Sci Rep* 2018;**8**:14035.

Hikita T, Miyata M, Watanabe R *et al. In vivo* imaging of long-term accumulation of cancer-derived exosomes using a BRET-based reporter. *Sci Rep* 2020;**10**:16616.

Jia X, Chen F, Pan W *et al.* Gliotoxin promotes *Aspergillus fumigatus* internalization into type II human pneumocyte A549 cells by inducing host phospholipase D activation. *Microbes Infect* 2014;**16**: 491–501.

Jia LJ, Rafiq M, Radosa L *et al. Aspergillus fumigatus* hijacks human p11 to redirect fungal-containing phagosomes to non-degradative pathway. *Cell Host Microbe* 2023;**31**:373–388.e10.

Józefowski S, Czerkies M, Łukasik A *et al.* Ceramide and ceramide 1-phosphate are negative regulators of TNF-α production induced by lipopolysaccharide. *J Immunol* 2010;**185**:6960–73.

Jun M-H, Jun Y-W, Kim K-H *et al.* Characterization of the cellular localization of C4orf34 as a novel endoplasmic reticulum resident protein. *BMB Reports* 2014;**47**:563–8.

Jurgielewicz BJ, Yao Y, Stice SL. Kinetics and specificity of HEK293T extracellular vesicle uptake using imaging flow cytometry. *Nanoscale Res Lett* 2020;**15**:170.

Kakarla R, Hur J, Kim YJ *et al.* Apoptotic cell-derived exosomes: messages from dying cells. *Exp Mol Med* 2020;**52**:1–6.

Köhler JR, Hube B, Puccia R *et al.* Fungi that infect humans. *Microbiol Spectr* 2017;**5**.

Kowal J, Arras G, Colombo M *et al.* Proteomic comparison defines novel markers to characterize heterogeneous populations of extracellular vesicle subtypes. *Proc Natl Acad Sci USA* 2016;**113**: E968–977.

Kulshreshtha A, Ahmad T, Agrawal A *et al.* Proinflammatory role of epithelial cell-derived exosomes in allergic airway inflammation. *J Allergy Clin Immunol* 2013;**131**:1194–203.

Latgé JP, Chamilos G. *Aspergillus fumigatus* and aspergillosis in 2019. *Clin Microbiol Rev* 2019;**33**:e00140–18.

Lázaro-Ibáñez E, Faruqu FN, Saleh AF *et al.* Selection of fluorescent, bioluminescent, and radioactive tracers to accurately reflect extracellular vesicle biodistribution *in vivo*. *ACS Nano* 2021;**5**: 3212–27

Levy D, Do MA, Brown A *et al.* Chapter one—genetic labeling of extracellular vesicles for studying biogenesis and uptake in living mammalian cells. In: Spada S, Galluzzi L (eds.), *Methods in Enzymology*. Cambridge, MA: Academic Press, 2020.

Lionakis MS, Drummond RA, Hohl TM. Immune responses to human fungal pathogens and therapeutic prospects. *Nat Rev Immunol* 2023;**23**:433–52.

Lischnig A, Bergqvist M, Ochiya T *et al.* Quantitative proteomics identifies proteins enriched in large and small extracellular vesicles. *Mol Cell Proteomics* 2022;**21**:100273.

Loconte L, Arguedas D, El R *et al.* Detection of the interactions of tumour derived extracellular vesicles with immune cells is dependent on EV-labelling methods. *J Extracell Vesicle* 2023;**12**:e12384.

Lőrincz Á M, Schütte M, Timár CI *et al.* Functionally and morphologically distinct populations of extracellular vesicles produced by human neutrophilic granulocytes. *J Leukoc Biol* 2015;**98**:583–9.

Lother J, Breitschopf T, Krappmann S *et al.* Human dendritic cell subsets display distinct interactions with the pathogenic mould *Aspergillus fumigatus*. *Int J Med Microbiol* 2014;**304**:1160–8.

Lötvall J, Hill AF, Hochberg F *et al.* Minimal experimental requirements for definition of extracellular vesicles and their functions: a position statement from the International Society for Extracellular Vesicles. *J Extracell Vesicle* 2014;**3**:26913.

Mathieu M, Névo N, Jouve M *et al.* Specificities of exosome versus small ectosome secretion revealed by live intracellular tracking of CD63 and CD9. *Nat Commun* 2021;**12**:4389.

Mondal A, Ashiq KA, Phulpagar P *et al.* Effective visualization and easy tracking of extracellular vesicles in glioma cells. *Biol Proced Online* 2019;**21**:4.

Morandi MI, Busko P, Ozer-Partuk E *et al.* Extracellular vesicle fusion visualized by cryo-electron microscopy. *PNAS Nexus* 2022;**1**:pgac156.

Mulcahy LA, Pink RC, Carter DR. Routes and mechanisms of extracellular vesicle uptake. *J Extracell Vesicle* 2014;**3**:25143819.

Myhill N, Lynes EM, Nanji JA *et al.* The subcellular distribution of calnexin is mediated by PACS-2. *MBoC* 2008;**19**:2777–88.

Paris S, Boisvieux-Ulrich E, Crestani B *et al.* Internalization of *Aspergillus fumigatus* conidia by epithelial and endothelial cells. *Infect Immun* 1997;**65**:1510–4.

Paskevicius T, Abou Farraj R, Michalak M *et al.* Calnexin, more than just a molecular chaperone. *Cells* 2023;**12**:403.

Perez-Riverol Y, Bai J, Bandla C *et al.* The PRIDE database resources in 2022: a hub for mass spectrometry-based proteomics evidences. *Nucleic Acids Res* 2022;**50**:D543–52.

Rafiq M, Rivieccio F, Zimmermann AK *et al.* PLB-985 neutrophil-like cells as a model to study *Aspergillus fumigatus* pathogenesis. *mSphere* 2022;**7**:e0094021.

Ricklefs FL, Maire CL, Reimer R *et al.* Imaging flow cytometry facilitates multiparametric characterization of extracellular vesicles in malignant brain tumours. *J Extracell Vesicle* 2019;**8**:1588555.

Ruf D, Brantl V, Wagener J. Mitochondrial fragmentation in *Aspergillus fumigatus* as early marker of granulocyte killing activity. *Front Cell Infect Microbiol* 2018;**8**:128.

Shopova IA, Belyaev I, Dasari P *et al.* Human neutrophils produce antifungal extracellular vesicles against *Aspergillus fumigatus*. *mBio* 2020;**11**:e00596–20.

Shpigelman J, Lao FS, Yao S *et al.* Generation and application of a reporter cell line for the quantitative screen of extracellular vesicle release. *Front Pharmacol* 2021;**12**:668609.

Slivinschi B, Manai F, Martinelli C *et al.* Enhanced delivery of Rose Bengal by amino acids starvation and exosomes inhibition in hu-

man astrocytoma cells to potentiate anticancer photodynamic therapy effects. *Cells* 2022;**11**:2502.

Strohmeier K, Hofmann M, Hauser F *et al.* CRISPR/Cas9 genome editing vs. over-expression for fluorescent extracellular vesicle-labeling: a quantitative analysis. *Int J Mol Sci* 2021;**23**:282.

Théry C, Witwer KW, Aikawa E *et al.* Minimal information for studies of extracellular vesicles 2018 (MISEV2018): a position statement of the International Society for Extracellular Vesicles and update of the MISEV2014 guidelines. *J Extracell Vesicle* 2018;**7**:1535750.

Timár CI, Lorincz AM, Csépányi-Kömi R *et al.* Antibacterial effect of microvesicles released from human neutrophilic granulocytes. *Blood* 2013;**121**:510–8.

Tognoli ML, Dancourt J, Bonsergent E *et al.* Lack of involvement of CD63 and CD9 tetraspanins in the extracellular vesicle content delivery process. *Commun Biol* 2023;**6**:532.

Trajkovic K, Hsu C, Chiantia S *et al.* Ceramide triggers budding of exosome vesicles into multivesicular endosomes. *Science* 2008;**319**:1244–7.

van de Veerdonk FL, Gresnigt MS, Romani L *et al.* *Aspergillus fumigatus* morphology and dynamic host interactions. *Nat Rev Microbiol* 2017;**15**:661–74.

van Niel G, D'Angelo G, Raposo G. Shedding light on the cell biology of extracellular vesicles. *Nat Rev Mol Cell Biol* 2018;**19**:213–28.

Verweij FJ, Balaj L, Boulanger CM *et al.* The power of imaging to understand extracellular vesicle biology *in vivo*. *Nat Methods* 2021;**18**:1013–26.

Wang S, He B, Wu H *et al.* Plant mRNAs move into a fungal pathogen via extracellular vesicles to reduce infection. *Cell Host Microbe* 2024;**32**:93–105.e6.

Welsh JA, Goberdhan DCI, O'Driscoll L *et al.* Minimal information for studies of extracellular vesicles (MISEV2023): from basic to advanced approaches. *J Extracell Vesicle* 2024;**13**:e12404.

WHO. *WHO Fungal Priority Pathogens List to Guide Research, Development and Public Health Action*, Vol. **48**. Geneva, 2022.

Willms E, Johansson HJ, Mäger I *et al.* Cells release subpopulations of exosomes with distinct molecular and biological properties. *Sci Rep* 2016;**6**:22519.

Yáñez-Mó M, Siljander PR, Andreu Z *et al.* Biological properties of extracellular vesicles and their physiological functions. *J Extracell Vesicle* 2015;**4**:27066.

Zhang X, He D, Gao S *et al.* iTRAQ–based proteomic analysis of the interaction of A549 human lung epithelial cells with *Aspergillus fumigatus* conidia. *Mol Med Rep* 2020;**22**:4601–10.

Zhang Z, Liu R, Noordhoek JA *et al.* Interaction of airway epithelial cells (A549) with spores and mycelium of *Aspergillus fumigatus*. *J Infect* 2005;**51**:375–82.

Received 16 April 2024; **revised** 16 October 2024; **accepted** 4 November 2024